# Accepted Manuscript

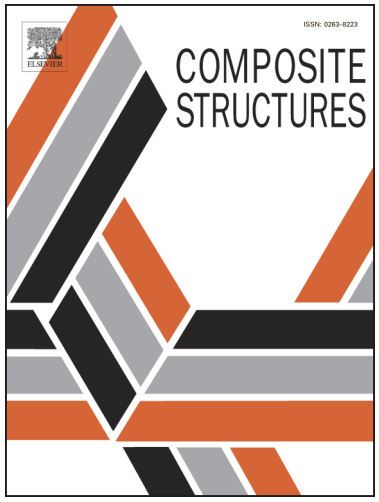


An extended cohesive damage model for simulating multicrack propagation in fibre composites

X. Li, J. Chen

PII: S0263-8223(16)30046-0
DOI: http://dx.doi.org/10.1016/j.compstruct.2016.02.026
Reference: COST 7238

To appear in: *Composite Structures*

Please cite this article as: Li, X., Chen, J., An extended cohesive damage model for simulating multicrack propagation in fibre composites, *Composite Structures* (2016), doi: http://dx.doi.org/10.1016/j.compstruct.2016.02.026

# An extended cohesive damage model for simulating multicrack propagation in fibre composites

X Li and J Chen*
School of Civil Engineering and Surveying, University of Portsmouth
Portland Street, Portsmouth PO1 3AH, UK

**Abstract**

This paper introduced an extended cohesive damage model (ECDM) for simulating multicrack propagation in fibre composites. The proposed ECDM is developed by introducing a cohesive damage model (CDM) into the eXtended Finite Element Method (XFEM) and eliminating the enriched degree of freedoms (DoFs) to effectively predict multicrack propagation in fibre composites without knowing beforehand the crack paths. A shifted Heaviside function is introduced to approximate existing cracks and crack propagations. A new strain field related cohesive damage law is introduced to describe the behaviour at the crack tip. The proposed ECDM is verified by three fracture test benchmarks and an example of predicting delamination migration together with matrix cracking. This investigation proved that the developed ECDM works very well when compared to analytical and experimental work. This developed ECDM supplies a novel numerical modelling approach for investigating multicrack failure mechanism in fibre composites.

**Keywords**: Extended cohesive damage model, Strain field related cohesive damage law, Multicrack, Composites

*Corresponding address: jiye.chen@port.ac.uk

## 1. Introduction

Carbon Fibre Reinforce Polymer (CFRP) composites have been commonly used in aerospace, shipbuilding and automobile engineering for several decades. Recently, the application of CFRP is increased in the constructional industry [1-2] and manufacture of sports instruments [3], etc. It is still challenging to fully understand the complex damage mechanism of fibre composites. With the extensive application of CFRP, the investigation of damage mechanisms of CFRP structures has been a major concern for the further development of CFRP in engineering structures. Currently there is a lack of reliable numerical approaches which provide engineers and researchers with efficient prediction for damage and failure when designing fibre composite structures. The Cohesive Damage Model (CDM), also known as Cohesive Zone Model (CZM), based on a Dudgale–Barenblatt cohesive zone approach [4, 5], is conducted for simulating crack propagation in the past two decades [6, 7]. The CDM can be used to describe the fracture behaviour of fibre composites including delamination and matrix cracking [8, 9]. However, the CDM approach has shortcomings because embedding corresponding interface elements is required in the zones where delamination is supposed to happen; it is difficult for the CDM to describe arbitrary matrix cracks in composites [6]. Moreover, the interface element with the CDM is insufficient in investigating some critical damage mechanisms, such as fibre fracture and kinking.

In the past decades, based on the partition of unity method (PUM), a rapid development has been made to characterize the arbitrary crack problem within

continuum solids [10-14]. In the PUM based approaches, the eXtended Finite Element Method (XFEM), as a combination of the classical Finite Element Method (FEM) and the PUM, originally introduced by Belytschko et al. [10] and subsequently enhanced by Moës et al. [15], is currently one of the most popular numerical approach utilized for the modelling of discontinuities in solids. By enriching the classical piecewise polynomial approximation basis within the finite element framework, the XFEM can thoroughly capture the discontinuities independently, including jumps, kinks, singularities, inhomogeneity, etc. [16].

Currently, one of the major challenges with regarding to damage prediction for heterogeneous materials, such as fibre composites, is that the most existing damage modelling approaches are incapable of presenting the complex failure mechanisms, such as multiple layered delamination and delamination migration. There are very few publications that have investigated this formidable problem [20-22]. To enable engineers and researchers to model the multicrack propagations in fibre composites, Chen has previously investigated the basic concept of combining the XFEM with the CDM without using a specified enriched item to cope with the singularity problem at the crack-tip [23] but additional enriched DoFs are employed to approximate existing cracks. The work presented in this paper is concerned with the development of the Extended Cohesive Damage Model (ECDM) based on the XFEM to simulate multicrack propagation without additional enriched DoFs required by the XFEM to improve computing efficiency through solving condensed equilibrium equations of

the ECDM; and pre-prepared crack path required by the CDM is no longer required by the ECDM.

The ECDM permits nodal displacement calculation of the cracked element in terms of standard degree of freedoms (DoFs) in FEM. The CDM is embedded into the ECDM to determine the damage initiation. The damage propagation is calculated by a new equivalent damage scale with respect to a strain field. The proposed ECDM with vigorous mathematic procedure fully covered the damage evolution from a weak discontinuity to a strong discontinuity. Different initial damage criterions and a linear softening damage law are introduced to address the characterization of multiple failure mechanisms in composites. Modelling of three fracture test benchmarks, involving double-cantilever-beam (DCB) for Mode I, end-notch-flexure (ENF) for Mode II and fixed ratio mixed mode (FRMM) for mixed-mode case are carried out to verify the proposed ECDM. As an example of modelling multi-layered delamination, delamination migration together with matrix cracking in a laminated composite specimen is simulated by the ECDM. This investigation proved the capability of the ECDM in prediction of multiple crack propagation in fibre composites.

## 2. The weak form of equilibrium equation

In fracture analysis, typical examples for strong and weak discontinuities are, respectively, cracks and interfacial difference between different domains or materials. The CDM, a traction-separation law is normally used to account for the singularity problem at the crack tip along the crack propagation path in which the cohesive

segment is embedded. Consider a 2D domain Ω with an outward normal vector **n** shown in Fig. 1, which is intersected by a cohesive crack $\Gamma_d$ with a normal vector **m**. Thus this domain Ω is divided into two subdomains presented by $\Omega^+$ and $\Omega^-$, respectively. The cohesive crack $\Gamma_d$ forms two internal boundaries $\Gamma^+_d$ and $\Gamma^-_d$. **t** is the cohesive force vector on the cohesive crack $\Gamma_d$, defined at the same direction with the normal vector **m**. The prescribed surface traction $\bar{\mathbf{t}}$ is imposed on boundary $\Gamma_t$. The prescribed displacement **u** is defined on boundary $\Gamma_u$. Omitting the body/volume forces, the strong form of the equilibrium equation can be written as:

$$\mathrm{Div}\,\boldsymbol{\sigma}=0 \tag{1}$$

Where **σ** is the Cauchy stress vector within the solid domain Ω. The boundary conditions for the domain Ω are:

$$\boldsymbol{\sigma}\cdot\mathbf{n}=\bar{\mathbf{t}} \ (\text{on } \Gamma_t), \quad \mathbf{u}=\bar{\mathbf{u}} \ (\text{on } \Gamma_u) \tag{2}$$

Because of the presence of cohesive segment, the boundary conditions imposed on the discontinuous boundary $\Gamma^+_d$ and $\Gamma^-_d$ should be:

$$\mathbf{t}^+=\boldsymbol{\sigma}^+\cdot\mathbf{n}^+=-\mathbf{t} \ (\text{on } \Gamma^+_d), \quad \mathbf{t}^-=\boldsymbol{\sigma}^-\cdot\mathbf{n}^-=\mathbf{t} \ (\text{on } \Gamma^-_d) \tag{3}$$

According to the traction-separation law, the traction known as cohesive force is a function of the relative displacement given by Equ. 4.

$$\mathbf{t}=\mathbf{t}(\delta) \tag{4}$$

Where δ is the relative displacement between two boundaries of the cohesive crack $\Gamma_d$. Equ. 4 serves as a nonlinear material model when discontinuity occurs.

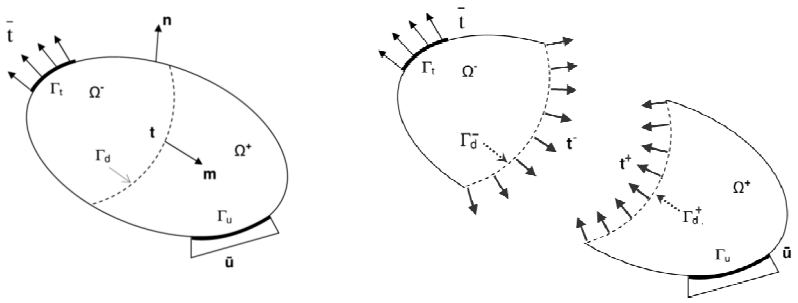


Fig. 1 Notation for a 2D domain with an arbitrary discontinuity $\Gamma_d$

While the cohesive forces/tractions are presented within the particular segment of a crack, the total potential of the body should take account of the contribution from cohesive tractions transferred through the crack surfaces. According to the principal of virtual work, the weak form of equilibrium equation can be obtained when introducing integration into the strong form (Equ. 1) as given below.

$$\int_{\Omega}\left[\nabla\boldsymbol{\omega}:\sigma(\mathbf{u})\right]d\Omega-\int_{\Gamma_t}\boldsymbol{\omega}\cdot\bar{\mathbf{t}}\,d\Gamma-\int_{\Gamma_d^+}\boldsymbol{\omega}\cdot\mathbf{t}^+\,d\Gamma-\int_{\Gamma_c^-}\boldsymbol{\omega}\cdot\mathbf{t}^-\,d\Gamma=0 \qquad (5)$$

In this weak form, $\boldsymbol{\omega}$ and $\mathbf{u}$ are respectively test displacement space and admissible displacement space in which we are seeking the solution.

## 3. Discrete form of equilibrium equation

The displacement field with "shifted" enrichment and without crack-tip enrichments is given by Equ. 6.

$$\mathbf{u}^h(\mathbf{x})=\sum_{i\in I}N_i(\mathbf{x})\mathbf{u}_i+\sum_{i\in J}N_j(\mathbf{x})\left(\mathrm{H}_{\Gamma_d}(\mathbf{x})-\mathrm{H}_{\Gamma_d}(\mathbf{x}_i)\right)\mathbf{a}_i \qquad (6)$$

Where $\mathbf{x}_i$ is the position coordinate for the $i_{th}$ node. $N_i$ is the conventional FEM shape functions associated with node $i$. $\mathbf{u}_i$ and $\mathbf{a}_i$ are the nodal variables associated with standard degree freedoms and enriched degree freedoms respectively at node $i$

and node *j*. The Heaviside step function $H_{\Gamma_d}$ shown in Equ. 7 can characterize the physical jump when material completely separates (strong discontinuities).

$$H_{\Gamma_d}(\mathbf{x}) = \begin{cases} 1 & \mathbf{x} \in \Omega^+ \\ 0 & \mathbf{x} \in \Omega^- \end{cases} \tag{7}$$

Where $\Omega^+$ is the one side domain from the discontinuity $\Gamma_d$, the $\Omega^-$ is another side domain. Using the Bubnov-Galerkin method, the trial functions and test function are chosen the same linear combination of interpolation functions as shown in Equ. 8. The discrete form of equilibrium equation for static analysis can be written as Equ. 8.

$$\begin{bmatrix} \mathbf{K}^{uu} & \mathbf{K}^{ua} \\ \mathbf{K}^{au} & \mathbf{K}^{aa} \end{bmatrix} \begin{bmatrix} \mathbf{u} \\ \mathbf{a} \end{bmatrix} = \begin{bmatrix} \mathbf{f}_{ext}^{u} \\ \mathbf{f}_{ext}^{a} \end{bmatrix} \tag{8}$$

Where $\mathbf{K}^{uu}$, $\mathbf{K}^{aa}$ and $\mathbf{K}^{ua}$ are the stiffness matrix associated with the standard FE approximation, the enriched approximation and the coupling between the standard FE approximation and the enriched approximation. $\mathbf{f}_{ext}^{\mathbf{u}}$ and $\mathbf{f}_{ext}^{a}$ are the equivalent nodal force vectors, $\mathbf{f}_{ext}^{u}$ is for standard FEM degrees of freedom while $\mathbf{f}_{ext}^{a}$ is for enriched degrees of freedom.

Assuming the crack shown in Fig. 1 is a cohesive crack, the discontinuous boundary is a cohesive crack boundary, i.e. $\Gamma_d = \Gamma_{coh}^{crack}$. In Equ. 8, the equivalent nodal force vectors without body force can be expressed as:

$$\begin{aligned} \mathbf{f}_{ext}^{u} &= \int_{\Gamma^h} \mathbf{N}^T \bar{\mathbf{t}} d\Gamma \\ \mathbf{f}_{ext}^{a} &= \int_{\Gamma^h} \mathbf{N}^T (H_{\Gamma_{coh}^{crack}}(x, y) - H_{\Gamma_{coh}^{crack}}(x_i, y_i)) \bar{\mathbf{t}} d\Gamma + \mathbf{f}_{coh} \end{aligned} \tag{9}$$

Where $\bar{\mathbf{t}}$ is the external nodal force vector as shown in Fig. 1. The internal nodal force vector due to cohesive force $\mathbf{t}$ on the crack surface $\Gamma_{coh}^{crack}$ can be expressed as:

$$\begin{aligned}\mathbf{f}_{coh} &= \int_{\Gamma_{coh}^{crack+}} \left(\mathrm{H}_{\Gamma_d}(x,y) - \mathrm{H}_{\Gamma_d}(x_i,y_i)\right)\mathbf{N}^T\mathbf{t}d\Gamma + \int_{\Gamma_{coh}^{crack-}} \left(\mathrm{H}_{\Gamma_d}(x,y) - \mathrm{H}_{\Gamma_d}(x_i,y_i)\right)\mathbf{N}^T(-\mathbf{t})d\Gamma \\ &= \int_{\Gamma_{coh}^{crack}} \mathbf{N}^T\mathbf{t}d\Gamma\end{aligned} \tag{10}$$

When damage increases, the cohesive traction decreases through a linear softening damage law shown in Fig. 2. Thus the traction **t** can be expressed as a function of a damage scale d, i.e., $\mathbf{t} = \mathbf{t_0}*(1\text{-}d)$ where $\mathbf{t}_0$ is the cohesive traction when crack propagates. It should be noted that there is not a physical relative displacement jump $\Delta\delta$ before a crack formed.

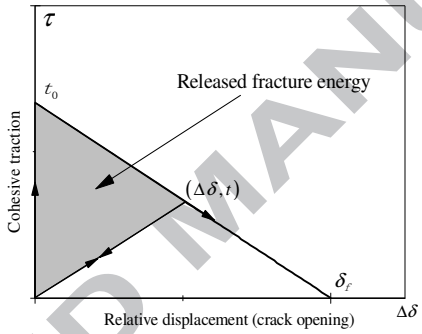


Fig. 2 A micromechanical linear softening damage law

## 4. Elimination of the enriched degree freedoms

With the purpose of reaching a fully condensed equilibrium system, we eliminate the additional enrichment term **a,** thus the equilibrium equation with the standard FEM unknown quantities can be consequently obtained as shown in Equ. 11.

$$\left(\mathbf{K}^{uu} - \mathbf{K}^{ua}\left(\mathbf{K}^{aa}\right)^{-1}\mathbf{K}^{au}\right)\mathbf{u} = \mathbf{f}_{ext}^{u} - \mathbf{K}^{ua}\left(\mathbf{K}^{aa}\right)^{-1}\mathbf{f}_{ext}^{a} - \mathbf{K}^{ua}\left(\mathbf{K}^{aa}\right)^{-1}\mathbf{f}_{coh} \tag{11}$$

It should be noticed that the sub-matrix $\mathbf{K}^{aa}$ is not necessarily invertible. In consideration of this feature, here the generalized inversed matrix (Moore–Penrose pseudoinverse) [17] is applied to complete the inversed matrix calculation in Equ. 11.

In order to simplify the problem, we suppose there is no distributed external load applied on the cracked element, then the evolved equilibrium equations with standard FEM degree freedoms can be simplified as shown in Equ. 12.

$$\left(\mathbf{K}^{uu}-\mathbf{K}^{ua}\left(\mathbf{K}^{aa}\right)^{-1}\mathbf{K}^{ua}\right)\mathbf{u}=\mathbf{f}_{ext}^{u}-\mathbf{K}^{ua}\left(\mathbf{K}^{aa}\right)^{-1}\mathbf{f}_{coh} \tag{12}$$

In the proposed ECDM, an equivalent damage scale is used to avoid the appearance of the enriched DoFs related displacement gap $\Delta\delta$. The strain energy released as shown in Fig. 2 due to the fracture should be equal to the released work done by cohesive traction. Therefore, the damage scale $d$ for cohesive behaviour along the crack can be expressed as below.

$$d=\frac{\int_{\Omega}\frac{1}{2}t_0\varepsilon d\Omega-\int_{\Omega}\frac{1}{2}t\varepsilon_0 d\Omega}{G_c l_{crack}} \tag{13}$$

Where $G_c$ is fracture energy; $l_{crack}$ is the length of a crack cutting the element, within which, the damage status is considered to be coincident. When $d$=1 the cohesive traction vanishes, and the cohesive crack evolves to a strong discontinuity (element separated). In Equ. 13, $t_0$ and $\varepsilon_0$ are, respectively, the initial traction or cohesive strength and the initial damage strain. As the softening constitutive law shown in Fig. 2 is used for reducing the cohesive traction, i.e. $t=(1-d)t_0$, we can achieve an explicit expression of the equivalent damage scale as shown below.

$$d=\frac{\int_{\Omega}\frac{1}{2}t_0\varepsilon d\Omega-\int_{\Omega}\frac{1}{2}t_0\varepsilon_0 d\Omega}{G_c l_{crack}-\int_{\Omega}\frac{1}{2}t_0\varepsilon_0 d\Omega} \tag{14}$$

Combining Equs. 10, 12 and 14 results the final condensed discrete form of equilibrium equation as shown in Equ. 15.

$$\left(\mathbf{K}_r^{uu}-\mathbf{K}_r^{ua}\left(\mathbf{K}_r^{aa}\right)^{-1}\mathbf{K}_r^{au}+\mathbf{K}_r^{ua}\left(\mathbf{K}_r^{aa}\right)^{-1}\left(\mathbf{L}_1-\mathbf{L}_2\right)\right)\mathbf{u}=\mathbf{f}_{ext}^{u} \tag{15}$$

In Equ. 15, the following two symbols are donated.

$$\mathbf{L}_1=\int_{\Gamma_{coh}^{crack}}\mathbf{N}^T t_0\frac{G_c l_{crack}}{G_c l_{crack}-\int_\Omega \frac{1}{2}t_0\varepsilon_0 d\Omega}d\Gamma\Re,\quad \mathbf{L}_2=\int_{\Gamma_{coh}^{crack}}\mathbf{N}^T t_0\frac{\int_\Omega \frac{1}{2}t_0\varepsilon d\Omega}{G_c l_{crack}-\int_\Omega \frac{1}{2}t_0\varepsilon_0 d\Omega}d\Gamma\Re \tag{16}$$

Where the operator $\Re$ for simplifying the final condensed equation is chosen as

$$\Re=\frac{1}{\left(\mathbf{K}_r^{ua}\left(\mathbf{K}_r^{aa}\right)^{-1}\int_{\Gamma_{coh}^{crack}}\mathbf{N}^T t_0 d\Gamma\right)^T\mathbf{u}}\left(\mathbf{K}_r^{ua}\left(\mathbf{K}_r^{aa}\right)^{-1}\int_{\Gamma_{coh}^{crack}}\mathbf{N}^T t_0 d\Gamma\right)^T \tag{17}$$

which satisfies $\Re\mathbf{u}=1$. It should be noticed that the Equ. 15 contains standard polynomial shape functions and conventional DoFs only, however, the left side of Equ. 15 is an actually equivalent stiffness matrix including the effects from enrichment and cohesive force.

## 5. Implementation and numerical Integration

The ECDM is programmed firstly as a user element through UEL in ABAQUS. Simulation of multicrack propagation such as delamination, matrix cracking and fibre breakage are considered in this investigation. Different damage criteria are used in the ECDM based FE analysis for judging different failure modes in the investigated composite samples. When simulating delamination and matrix cracking, a stress based criteria and an equivalent damage scale based criteria are used for judging the damage

initiation and crack propagation respectively. A maximum principal stress based criteria is used to characterize the fibre's rupture, which means when the maximum principal stress $\sigma_{max}$ at Gauss points of relevant elements is beyond the fibre strength $S_{fibre}$, the fibre breakage occurs.

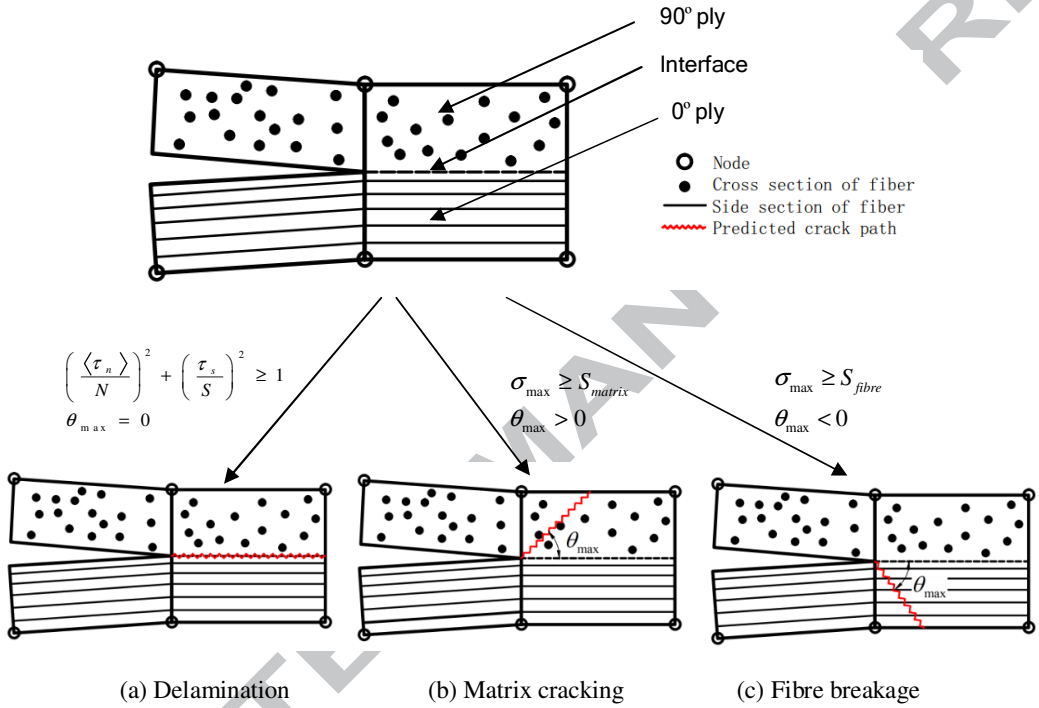


(a) Delamination (b) Matrix cracking (c) Fibre breakage

Fig. 3 Schematic failure modes and their initial judgements

Fig. 3 schematically illustrates three fracture modes in composites, delamination, matrix cracking and fibre breakage. Fig. 3 also gives initial judgement criteria to determine the mode of fracture. The stresses taken from the mid-point of the interface within corresponding elements are used in the judgement of delamination initiation. The damage scale *d* given in Equ. 13 is used to account for delamination propagation. Meanwhile, the average maximum principal stress taken from four Gauss points of the elements at upper layer (90° ply) and lower layer (0° ply) are used in the

judgements for matrix crack and fibre breakage, respectively. The crack directions of matrix fracture and fibre breakage are determined by the direction $\theta_{\max}$ which is perpendicular to the maximum principal stress. Newton-Raphson method together with line search scheme is employed for the non-linear iteration when solving Equ. 15. In order to improve the convergence in damage propagation regime, the viscous regularization scheme [18] is employed which can significantly speed up the simulation process.

## 6. Validation of the ECDM

### 6.1 Benchmark specimens

In this section, three benchmark specimens regarding single mode and mixed mode delamination are investigated to verify the performance of the developed ECDM. The loading and boundary conditions and geometric dimensions of specimens are illustrated in Fig. 4. The fracture modes studied are mode I via Double Cantilever Beam (DCB) test (Fig. 4a), mode II via End Notched Flexure (ENF) test (Fig. 4b) and Mixed-mode via Fixed Ratio Mixed Mode (FRMM) test (Fig. 4c). The elastic material properties for each lamina and fracture properties are given in Table 1 together with detailed geometric dimensions of specimen in which $w$ denotes the out-of-plane width of specimen.

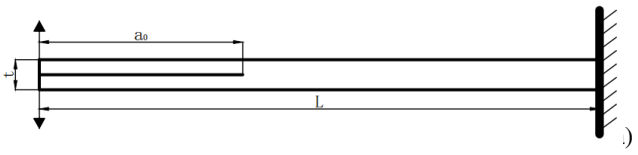

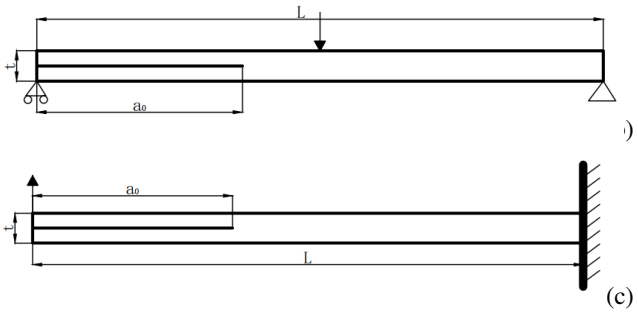


Fig. 4 Benchmark specimen configurations: (a) DCB, (b) ENF and (c) FRMM

Table 1 Dimensions and material parameters of benchmark specimen

| Specimen | $E_{11}$ | $E_{22}$ | $G_{12}$ | $v$ | $\tau_n$ | $\tau_s$ | $G_{Ic}$ | $G_{IIc}$ | L | B | w | $a_0$ |
|---|---|---|---|---|---|---|---|---|---|---|---|---|
| | (GPa) | | | | (MPa) | | (J/mm$^2$) | | (mm) | | | |
| DCB | 130 | 8 | 6 | 0.27 | 48 | 48 | 0.256 | 0.784 | 105 | 3.1 | 24 | 22 |
| ENF | 122.7 | 10.1 | 5.5 | 0.25 | 100 | 100 | N/A | 1.719 | 102 | 3.12 | 25.4 | 39.3 |
| FRMM | 130 | 8 | 6 | 0.27 | 48 | 48 | 0.256 | 0.784 | 105 | 3.1 | 24 | 45 |

### 6.2 Results of benchmark modelling

***DCB.*** The mode I delamination propagation is shown in Fig. 5, which symmetrically went through the mid-plane of DCB specimen. The elements with grey colour indicate the delamination propagation. The reaction force on loading point is calculated when the algorithm satisfied the convergent criteria. The predicted load-displacement relationship is given in Fig. 6 in which an analytical solution is also given by the corrected beam theory (Appendix A.1) for comparison. It can be seen that the overall load-deflection solution obtained by the ECDM has a good agreement with the analytical solution. It can be seen from Fig. 6 that the elastic loading bearing response (OB) can be observed, followed by the post failure response (BC) which

represents the propagation of model I delamination. The ECDM predicted post failure response is slightly higher than analytical solution.

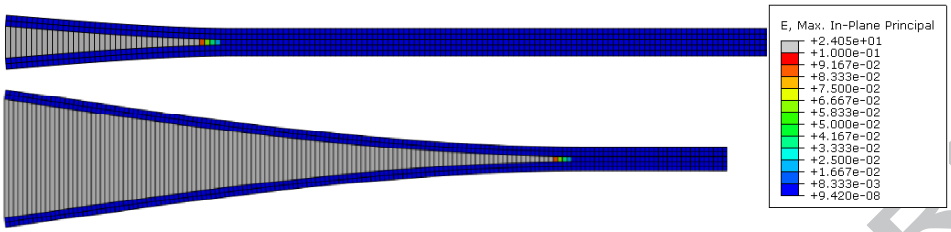


Fig. 5 Simulated mode I delamination propagation and strain contours

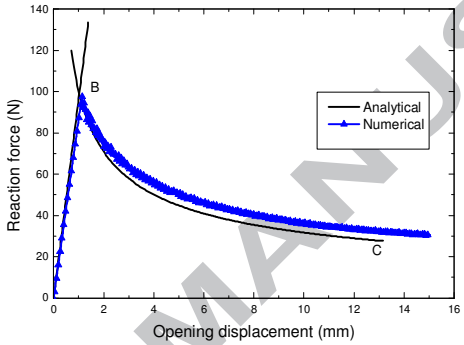


Fig. 6 The ECDM predicted failure response of DCB and analytical solution

***ENF.*** The corresponding experimental work of ENF is given by Paul et.al [19]. Fig. 7 shows the ECDM simulated mode II delamination together with the corresponding maximum principal strain filed. Fig. 8 shows the ECDM predicted load-deflection curve together with the analytical and experimental solution. It can be seen from Fig. 8 that when applying displacement around 2.56 mm the delamination starts, the corresponding reaction force is about 485 N. In general, the ECDM predicted post failure response agrees the analytical solution well, and is between the analytical solution (Appendix A.2) and experimental measurement. It should be noted that the experimental measurement is unstable in the post failure stage.

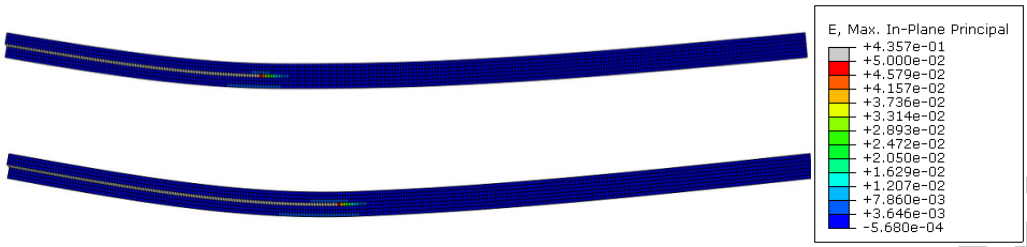


Fig.7 Simulated mode II delamination propagation and strain contours

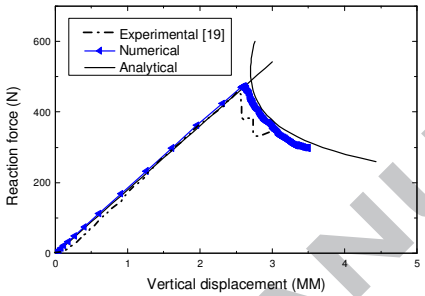


Fig. 8 The predicted failure response of ENF together with analytical and experimental results

***FRMM.*** The final benchmark example is an FRMM test in which a displacement loading is applied at the one end of upper cantilever beam with an initial delamination. Fig. 9 shows the ECDM simulated mixed-mode delamination propagation and corresponding strain contours. The predicted load-displacement curve is shown in Fig. 10 together with analytical and experimental measurement. It can be seen from Fig. 10 that the ECDM prediction agrees with analytical and experimental results very well in both elastic stage (line OB) and post failure stage (curve BC). The analytical solution of FRMM is given by the corrected beam theory (Appendix A.3), and corresponding test result is taken from [8].

## 7. Modelling of delamination migration

Most previous modelling investigations on delamination propagation focused on the delamination at a single interlaminar interface. Actually, the damage in composite laminates often involves multiple layered delaminations, which normally grow and migrate into different interlaminar interfaces. The publications [20-23] highlighted the great concern of constructing a powerful numerical model with the capability of modelling multiple failure mechanisms including delamination migration, matrix cracking and fibre breakage. The proposed ECDM with arbitrary crack characterization and avoidance of pre-prepared crack path in FE mesh is believed to be suitable for modelling multicrack behaviour in composites. Herein, a typical delamination migration problem together with a matrix crack in a laminated composite specimen is investigated using the ECDM to validate the capability of the ECDM in predicting the multiple layered delamination together with matrix cracking.

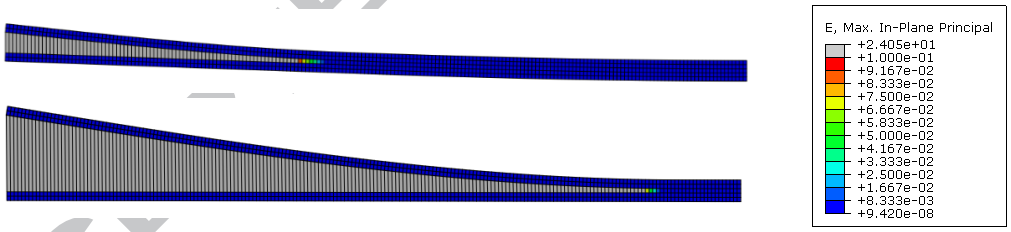


Fig. 9 The ECDM simulated mixed-mode delamination propagation and strain contours

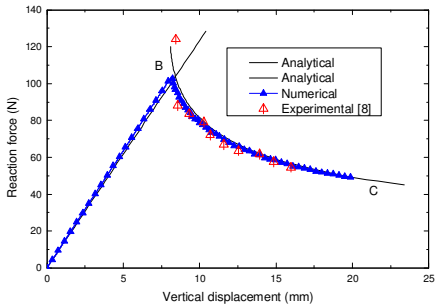


Fig. 10 The predicted failure response of FRMM together with analytical and experimental results

The configuration of test specimen consists of a cross-ply IM7/8552 tape laminate with a polytetrafluoroethylene insert implanted at the mid-plane and spanning part way along the length of the specimen. The detailed configuration as well as the test set-up of specimen can be referred to [20]. The lay-up sequence of the laminate is $[90_4/0_3/(90/0)_{2s}/0_3/90_4/T/0/90_4/0/0/(90/0)_{2s}/0/0/90_3/0/90]$. The material properties of IM7/8552 lamina are $E_{11}$=161.0Gpa, $E_{22}=E_{33}$=11,38Gpa, $v_{12}=v_{13}$=0.32 $v_{23}$=0.436 $G_{12}=G_{13}$=5.17Gpa and $G_{23}$=3.98Gpa, respectively. The dimensional unit used in Fig. 11 is mm, the width of specimen is 12.7 mm.

Following up experimental work, a pre-existing delamination with the length of 51mm at the 0/90 interlaminar interface is embedded in the FE mesh. A vertical displacement is applied at the existing crack tip to initiate delamination onset and propagation, and to lead the matrix cracking through the 90-degree ply followed by a migration of the delamination to a neighbouring 90/0 interlaminar interface. Fig. 12 shows the ECDM simulated a final failure stage with delamination growth, matrix crack and delamination migration.

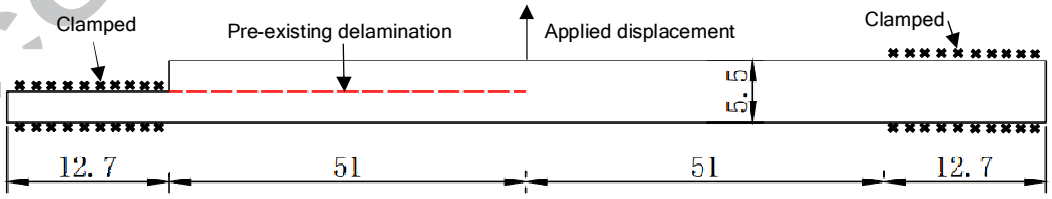


Fig. 11 The configuration of delamination migration test

The global failure response of the investigated specimen is shown in Fig.13, from which it can be seen that the entire failure response obtained from the modelling is

sufficiently consistent with experimental measurements. The failure response of the specimen experienced three sudden drops during the loading process, which represent three fractures regarding delamination growth, matrix crack and delamination migration respectively. When the specimen is loaded over 200N, the delamination propagated approximately 8.6mm along the 0/90 intralaminar interface, which agrees to the experimental observation between 8 and 9mm. This delamination is an unstable delamination propagation at the 0/90 interface and is reflected by the first response drop shown in Fig. 13. When the specimen is reloaded up between 150N and 175N, a matrix crack stated and unstably went through the 90-degree ply along a slope line from the bottom to top of 90-degree ply, which is reflected by the second response drop. When the response dropped down to the value between 100N and 125N, the response is a short flat stage then followed by the third response drop which is relatively smooth and downward. The third drop related response is actually another delamination as a stable crack propagation at the 90/0 interlaminar interface, which is finally followed by the residual stiffness of the specimen. This multicrack propagation actually presented the delamination migration through a matrix crack in the investigated specimen. Prior to and after delamination migration it is recognized the fracture is mixed mode-I/II crack due to the asymmetrical load condition and specimen configuration. Inspection of the kinked surface in 90-degree ply of tested specimen [22] revealed the mode-I fracture, which proved the modelling prediction of the opening dominated matrix crack. It should be noticed that the transition of the

kinked crack from 0/90 interface into the 90/0 interface is sudden which is reflected by a short gap between the second and third drop in the failure response shown in Fig. 13. This is possibly because a considerable amount of strain energy is attained within 90-degree ply prior to the delamination migration. This investigation confirmed that the capability of the ECDM in capturing the entire delamination migration path including both interlaminar fracture and intralaminar crack propagation in the investigated laminated composite specimen.

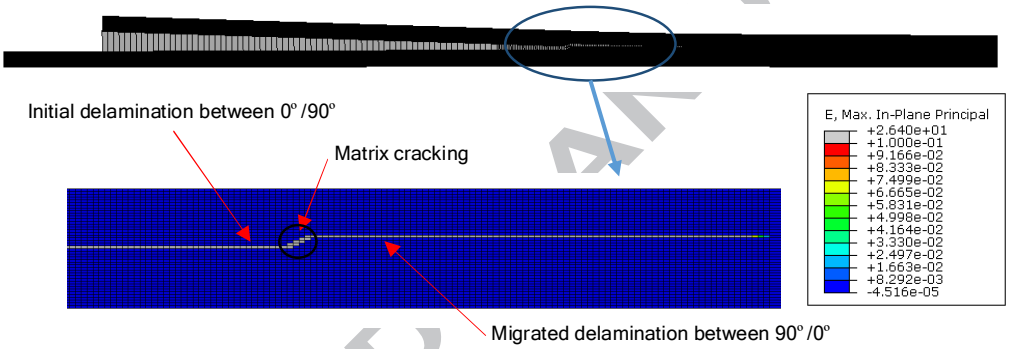


Fig.12 The ECDM simulated delamination migration together with a matrix crack

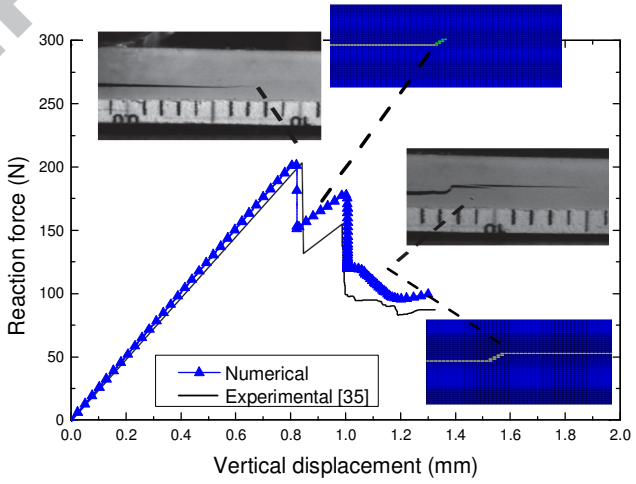


Fig. 13 The load-displacement curves given by the ECDM and experimental measurement

## 8. Conclusion and future work

The basic equilibrium equation of the ECDM without additional enriched DoFs is achieved to efficiently simulate multicrack propagation in fibre composites. An equivalent damage scale relating to strain field is introduced to avoid enriched DoFs in calculation of crack related displacement jump. Comparing to the XFEM and CDM, the ECDM is able to account for multicrack propagation within an element, and pre-prepared crack paths are no longer required. This advantage enables the ECDM to model multicrack propagation such as matrix crack, delamination and fibre breakage in laminated composites. With this approach, a comprehensive numerical prediction of failure mechanism in fibre composites can be completed with less computational endeavour. Considering the length of this paper, detailed computing efficiency of the ECDM will be discussed in different articles.

This developed novel ECDM is implemented using the user subroutine UEL in the commercial finite element package ABAQUS. This proposed ECDM has been verified by three fracture benchmark specimens and a laminated composite sample. By the benchmark examples, it indicated that the ECDM is capable to simulate single mode delamination as well as the mixed mode delamination with sufficient accuracy. The laminated composite sample with delamination migration together with matrix cracking validated the capability of the ECDM in predicting multicrack failure including multiple layered delamination and matrix cracking without using pre-prepared crack paths. This developed ECDM provides a new modelling approach

for engineers and researchers to investigate detailed multicrack failure mechanism in fibre composites. The future work will include three dimensional modelling simulation of multicrack propagation using the ECDM, and applying the ECDM in multiscale modelling to investigate the micro and macro damage failure mechanism in fibre composites.

**Reference**


[1] Bakis CE, Bank LC, Brown VL, et al. Fiber-reinforced polymer composites for construction-state-of-the-art review. J Compos 2002; 6(2):73–87.

[2] Gao, Y., Chen, J., Zhang, Z., & Fox, D. An advanced FRP floor panel system in buildings. Composite Structures 2013; 96: 683-690.

[3] Subic, A. Materials in sports equipment (Vol. 2). Elsevier 2007.

[4] Barenblatt GI. The formation of equilibrium cracks during brittle fracture. General ideas and hypotheses: axially symmetric cracks. Journal of Applied Mathematics and Mechanics (PMM) 1959; 23:434–444.

[5] Dugdale DS. Yielding of steel sheets containing slits. Journal of the Mechanics and Physics of Solids 1960; 8:100–104.

[6] Elices, M., Guinea, G. V., Gomez, J., & Planas, J. The cohesive zone model: advantages, limitations and challenges. Engineering fracture mechanics 2002; 69(2): 137-163.

[7] He, X. A review of finite element analysis of adhesively bonded joints. International Journal of Adhesion and Adhesives 2011; 31(4): 248-264.

[8] Chen, M. Crisfield, AJ Kinloch, EP Busso, FL Matthews, Y. Qiu, J. Predicting progressive delamination of composite material specimens via interface elements. Mechanics of composite materials and structures 1999; 6(4): 301-317.

[9] Hallett, S. R., Jiang, W. G., Khan, B., & Wisnom, M. R. Modelling the interaction between matrix cracks and delamination damage in scaled quasi-isotropic specimens. Composites Science and Technology 2008; 68(1): 80-89.

[10] Belytschko, T. & Black, T., Elastic crack growth in finite elements with minimal remeshing. International Journal for Numerical Methods in Engineering 1999; 45: 601-620.

[11] Duarte, C. A., Hamzeh, O. N., Liszka, T. J., & Tworzydlo, W. W., A generalized finite element method for the simulation of three-dimensional dynamic crack propagation. Computer Methods in Applied Mechanics and Engineering 2001; 190(15): 2227-2262.

[12] Oden, J. T., Duarte, C. A. M., & Zienkiewicz, O. C., A new cloud-based hp finite element method. Computer methods in applied mechanics and engineering 1998; 153(1): 117-126.

[13] Glowinski, R., He, J., Rappaz, J., & Wagner, J., Approximation of multi-scale elliptic problems using patches of finite elements. Comptes Rendus Mathematique 2003; 337(10): 679-684.

[14] Strouboulis, T., Babuška, I., & Hidajat, R., The generalized finite element method for Helmholtz equation: theory, computation, and open problems. Computer Methods in Applied Mechanics and Engineering 2006; 195(37): 4711-4731.

[15] Moës, N, Dolbow, J, & Belytschko, T., A finite element method for crack growth without remeshing. International Journal for Numerical Methods in Engineering 1999; 46(1): 131-150.

[16] Belytschko, T., Gracie, R., & Ventura, G. A review of extended/generalized finite element methods for material modeling. Modelling and Simulation in Materials Science and Engineering 2009; 17(4): 043001.

[17] Wang, G., Wei, Y., Qiao, S., Lin, P., & Chen, Y., Generalized inverses: theory and computations. Beijing Science Press 2004: 37-75.

[18] Duvaut G, Lions JL. Inequalities in mechanics and physics. Berlin: Springer 1976.

[19] Harper, P. W., & Hallett, S. R. Cohesive zone length in numerical simulations of composite delamination. Engineering Fracture Mechanics 2008; 75(16): 4774-4792.

[20] Ratcliffe, J. G., Czabaj, M. W., & O'Brien, T. K. Characterizing delamination migration in carbon/epoxy tape laminates. National Aeronautics and Space Administration Technical Memorandum, NASA/TM – 2013–218028; 2013.

[21] Ratcliffe, J. G., & DeCarvalho, N. V. Investigating delamination migration in composite tape laminates. National Aeronautics and Space Administration Technical Memorandum, NASA/TM – 2014–218289; 2014.

[22] Pernice, M. F., De Carvalho, N. V., Ratcliffe, J. G., & Hallett, S. R. Experimental study on delamination migration in composite laminates. Composites Part A: Applied Science and Manufacturing 2015; 73: 20-34.

[23] J. Chen, An extended cohesive damage model with a length scale in fracture analysis of adhesively bonded joints, Engineering Fracture Mechanics 2014; 119: 202–213.

[24] Blackman, B. R. K., Hadavinia, H., Kinloch, A. J., Paraschi, M., & Williams, J. G. The calculation of adhesive fracture energies in mode I: revisiting the tapered double cantilever beam (TDCB) test. Engineering Fracture Mechanics 2003; 70(2): 233-248.

[25] Reeder, James R., Kevin Demarco, & Karen S. Whitley. The use of doubler reinforcement in delamination toughness testing. Composites Part A: Applied Science and Manufacturing 2004; 35(11): 1337-1344.

[26]Hodgkinson, John M., Mechanical testing of advanced fibre composites, Elsevier, 2000.

**Appendix: The corrected beam theory for DCB, ENF and FRMM**

In the corrected beam theory, the beam is assumed to be linear elastic. The foundation of the method is based on Irwin–Kies equation in the framework of linear elastic fracture mechanics. In a linear structure system, the fracture energy is given by [24]:

$$Gc = \frac{F^2}{2b}\frac{\partial C}{\partial a} \qquad \text{(a-1)}$$

Where $C$ is the compliance of the beam expressed as $C=\Delta/F$, $a$ is the crack length and $b$ is the out-of-plane width of beam. The calculation and measurement of the differentiation of the compliance is varied for different configurations.

A.1. Mode I DCB

Considering the unidirectional DCB specimen shown in Fig. 4a as a double cantilever beam, assume the adherents are strictly clamped at crack tip of initial delamination. Euler-Bernoulli beam theory can be applied to calculate the vertical separation at the end of double cantilever beam [25]:

$$\Delta = \frac{2F\left(a+\chi h\right)^3}{3E_{11}I} \qquad \text{(a-2)}$$

Where I is the second moment of the area of the double cantilever beam, $E_{11}$ is the Yong's modules in length direction, h is the half thickness of the double cantilever beam, $\chi h$ is the term of correcting crack length in order to correct the displacement for shear deformation and local deformation that occurs around the crack tip. Substituting the corrected displacement expression into the basic fracture energy formula (a-1) results a concise expression of mode I fracture energy as:

$$G_{I,c} = \frac{F^2 (a+\chi h)^2}{EbI} = \frac{12F^2 (a+\chi h)^2}{Eb^2 h^3} \quad \text{(a-3)}$$

The correction parameter $\chi$ depends on the elastic parameters of the material, which can be calculated as:

$$\chi = \sqrt{\frac{E_{11}}{11G_{13}}\left[3 - 2\left(\frac{1.18\sqrt{E_{11}E_{22}}/G_{13}}{1+1.18\sqrt{E_{11}E_{22}}/G_{13}}\right)^2\right]} \quad \text{(a-4)}$$

A.2 Mode II ENF

The basically same formula given in (a-1) can be applied for the ENF (see Fig. 4b), in which the displacement and mode II strain energy release rate before crack propagation can be calculated as [25]:

$$\Delta = \frac{3F(\mathrm{a}+0.42\chi h)^3 + 2FL^3}{96E_{11}I} \quad \text{(a-5)}$$

$$G_{II,c} = \frac{3F^2 (a+0.42\chi h)^2}{64E_{11}bI} = \frac{9F^2 (a+0.42\chi h)^2}{16E_{11}b^2 h^3} \quad \text{(a-6)}$$

A.3 Mixed mode FRMM

The configuration of FRMM is shown in Fig. 4c. A constant ration between mode I and mode II is assumed. The tip displacement of the upper cantilever beam can be given by the following equation [26]:

$$\Delta = N' \frac{F\left(7(a+0.42\chi h)^3 + (L+2\chi h)^3\right)}{2E_{11}bh^3} \quad \text{(a-7)}$$

*N'* is the correction factor of the compliance and can be calculated as:

$$N' = 1 - \left(\frac{l_2}{a}\right)^3 - \frac{9}{8}\frac{\delta l_1}{a^2}\left[1 - \left(\frac{l_2}{a}\right)^2\right] - \frac{9}{35}\left(\frac{\delta}{a}\right)^2 \quad \text{(a-8)}$$

Where $l_1$ is the distance from the centre of the loading block to the mid-plane of the specimen; $l_2$ is the half length of the loading block. It should be noted that the loading block is applied on the top surface at the end of the specimen.

The total fracture energy leading mixed mode crack propagation can be expressed as:

$$G_c^{total} = G_I + G_{II} \quad \text{(a-9)}$$

The calculation of two individual components in mixed mode fracture, $G_I$ and $G_{II}$, can be obtained respectively as:

$$G_I = \psi \frac{3F^2\left(a + \chi h\right)^2}{E_{11} b^2 h^3} \quad \text{(a-10)}$$

$$G_{II} = \psi \frac{9F^2\left(a + 0.42\chi h\right)^2}{4E_{11} b^2 h^3} \quad \text{(a-11)}$$

Where ψ is the correction factor for large displacement and end block effect, and given by:

$$\psi = 1 - \theta_1\left(\frac{\Delta}{L}\right) - \theta_2\left(\frac{\Delta l_1}{L^2}\right) \quad \text{(a-12)}$$

in which

$$\theta_1 = \frac{1101\left(\frac{a}{L}\right)^4 + 390\left(\frac{a}{L}\right)^2 + 45}{140\left(\frac{a}{L}\right)^3 + 20}$$

$$\theta_2 = 3\left(\frac{a}{L}\right)\frac{7\left(\frac{a}{L}\right)^2 + 1}{7\left(\frac{a}{L}\right)^3 + 1} \quad \text{(a-13)}$$